

Necrotic cell sensor Clec4e promotes a pro-atherogenic macrophage phenotype through activation of the unfolded protein response

Clément, Necrotic sensor Clec4e promotes atherosclerosis

Marc Clément, PhD^{1*}, Gemma Basatemur, PhD^{1*}, Leanne Masters, BS¹, Lauren Baker, BS¹, Patrick Bruneval, MD², Takao Iwawaki, PhD³, Manfred Kneilling, MD^{4,5}, Sho Yamasaki, PhD⁶, Jane Goodall, PhD¹, Ziad Mallat, MD, PhD^{1,2}

¹Division of Cardiovascular Medicine, University of Cambridge, Cambridge, UK.

²Institut National de la Santé et de la Recherche Médicale, Paris Cardiovascular Research Center, Paris, France

³Iwawaki lab, Advanced Scientific Research Leaders Development Unit, Gunma University, Maebashi, Gunma, Japan

⁴Department of Preclinical Imaging and Radiopharmacy, Werner Siemens Imaging Center, Eberhard Karls University, Tübingen, Germany

⁵Department of Dermatology, Eberhard Karls University, Tübingen, Germany

⁶Division of Molecular Immunology, Medical Institute of Bioregulation, Kyushu University, Japan

Correspondence should be addressed to: Ziad Mallat, MD, PhD, at Division of Cardiovascular Medicine, University of Cambridge, Addenbrooke's Hospital,

CIRCULATIONAHA/2016/022668-R1

Cambridge, CB2 2QQ, UK. Tel: +44 1223 768678; Fax: +44 1223 746962; E-Mail: zm255@medchl.cam.ac.uk.

*Equal contribution.

Total word count: 6999.

Journal Subject Codes:

Basic, Translational, and Clinical Research: Basic Science Research;

Inflammation; Lipids and Cholesterol; Pathophysiology.

Vascular Disease: Atherosclerosis.

Abstract

Background—Atherosclerotic lesion expansion is characterized by the development of a lipid rich necrotic core known to be associated with the occurrence of complications. Abnormal lipid handling, inflammation, and alteration of cell survival or proliferation contribute to necrotic core formation, but the molecular mechanisms involved in this process are not properly understood. Clec4e receptor recognizes the cord factor of *M. Tuberculosis*, but also senses molecular patterns released by necrotic cells, and drives inflammation.

Methods—We hypothesized that activation of Clec4e signaling by necrosis is causally involved in atherogenesis. We addressed the impact of Clec4e activation on macrophage functions in vitro, and on the development of atherosclerosis using low-density lipoprotein receptor deficient (*Ldlr*^{-/-}) mice in vivo.

Results—We show that Clec4e is expressed within human and mouse atherosclerotic lesions, and is activated by necrotic lesion extracts. Clec4e signaling in macrophages inhibits cholesterol efflux and induces a Syk-mediated endoplasmic reticulum (ER) stress response, leading to the induction of pro-inflammatory mediators and growth factors. *Chop* and *Ire1a* deficiencies significantly limit Clec4e-dependent effects, whereas *Atf3* deficiency aggravates Clec4e-mediated inflammation and alteration of cholesterol efflux. Repopulation of *Ldlr*^{-/-} mice with *Clec4e*^{-/-} bone marrow reduces lipid accumulation, ER-stress, macrophage inflammation and proliferation within the developing arterial lesions, and significantly limits atherosclerosis.

Conclusions—Our results identify a non-redundant role for Clec4e in coordinating major biological pathways involved in atherosclerosis, and suggest that it may play similar roles in other chronic inflammatory diseases.

Key words: necrosis; proliferation; inflammation; atherosclerosis.

Clinical Perspective

What is new?

- Necrosis is a major feature of advanced atherosclerotic plaques. Moreover, increased size of necrotic lipid core is an important risk factor of plaque instability. Here we show that sensing of necrotic cells by the C-type lectin receptor CLEC4E orchestrates major pathophysiological events during plaque development and progression. CLEC4E signaling in macrophages uniquely coordinates the inflammatory response with lipid handling, foam cell formation, and cell proliferation, and promotes the development of advanced atherosclerotic lesions.
- We also uncover a critical role for the unfolded protein response in mediating pro-atherogenic macrophage functions downstream of CLEC4E.

What are the clinical implications?

- The present work provides a mechanistic explanation for the close association between necrotic lipid core formation and the development of inflammatory advanced atherosclerotic lesions.
- It will be important to examine if increased CLEC4E expression/signaling is associated with the formation of thin-cap fibroatheromatous lesions, and if blockade of CLEC4E signaling is able to promote plaque stabilization.

Surprising similarities exist between the formation of advanced atherosclerotic lesions and tuberculous granulomas. These are both characterized by the presence of a necrotic lipid core, covered, in atherosclerotic plaques by a fibrous cap, and in granulomas by a fibrous capsule.

In atherosclerosis, increased necrotic core size and accumulation of inflammatory cells, alongside reduced fibrous cap thickness, are important determinants of acute ischemic cardiovascular events (acute myocardial infarction and sudden death). Necrotic core development is initiated by the formation of macrophage- and smooth muscle cell-derived foam cells in response to the accumulation of oxidized lipoproteins in the arterial wall and the activation of pattern recognition innate immune receptors¹. An acellular necrotic core is then established as defective efferocytosis (clearance of apoptotic cells) leads to secondary necrosis of foam cells and accumulation of cell debris¹.

In granulomas, lipid body formation occurs in mycobacterium infected macrophages, and may result from both mycobacterium-derived (oxygenated mycolic acids) and host-derived lipids². The core of the granuloma accumulates necrotic debris from dead cells, and cholesterol crystals, which induce further inflammation and contribute to granuloma remodeling³. Formation of inflammatory foamy macrophages appears to be driven at least in part by the mycobacterium cell wall lipid trehalose-6, 6'-dimycolate (TDM)⁴. Until now, the underlying mechanism for this has been attributed to potential recognition of

TDM by Toll-like receptor (TLR)2, operating in concert with the scavenger receptor MARCO^{4,5}. However recently, the C-type lectin receptors (Clec)4e and 4d have been identified as bona fide receptors for TDM^{6,7}, thus implicating Clec4e and Clec4d in the events leading to granuloma formation.

Clec4d is coupled with Clec4e, and essentially promotes Clec4e cell surface expression and signaling⁷. Clec4e (also known as Mincle), is an ITAM-coupled FcR γ -dependent signaling receptor, that initiates signaling by binding Syk through its Src homology 2 domain⁸. Interestingly, Clec4e not only recognizes mycobacterial derived mycolate-containing lipid species (TDM, and glycerol monomycolate)^{6,9}, but also senses host cell damage through the recognition of SAP130, a nuclear ribonucleoprotein released during necrotic cell death⁸. This places Clec4e at the center of events in granuloma formation and, by analogy, is highly suggestive of a role for Clec4e signaling in the molecular events at play in advanced atherosclerotic lesions. Therefore, we tested the hypothesis that Clec4e signaling promotes atherosclerosis.

Methods

Detailed methods can be found in the online-only Data Supplement.

Animals. Experiments were approved by the Home Office, UK. *Clec4e*^{-/-}¹⁰, *Chop*^{-/-} (Jackson laboratories), *Irf1a*^{flox/flox}¹¹, ERAI¹² and *Atf3*^{-/-}¹³ mice were previously described. Male 6-8 week old *Ldlr*^{-/-} mice were lethally irradiated (9.5 Gy) then injected i.v. with 1x10⁷ bone marrow cells from donor mice. After 4

weeks recovery, mice were fed a high fat diet for 20 weeks. Littermate *Clec4e*^{+/+}, *Clec4e*^{-/-} mice were used as donors for bone marrow transfer.

Extent and composition of atherosclerotic lesions. Quantification of lesion size and composition was performed as previously described ¹⁴.

Cell culture. Where indicated, cells were pre-incubated with Syk inhibitor (5 μ M, R406; Selleckchem) or Ire1 α inhibitor (25 μ M, STF-083010; Calbiochem), and treated with Tunicamycin (1 μ g/ml, Sigma), thapsigargin (1 μ M, Sigma), anti-Csf1 (10 μ g/ml, R&D systems, clone 131621), rat IgG (10 μ g/ml, R&D system; 6-001-F), TDB (50 μ g/ml, 22:0 Trehalose; D-(+)-trehalose 6,6'-dibehenate, Avanti® polar lipids inc. purity >99%). BMDM proliferation was estimated by MTT assay (Sigma, CGD1-1KT).

Cholesterol efflux was measured by an assay kit (MAK192, Sigma). BMDMs were stimulated for 24 hours with oxLDL (50 μ g/ml) and TDB (10 μ g/ml) in complete medium. Cells were washed and incubated with human purified HDL (Abserotec, 50 μ g/ml), mouse serum (Sigma, 5% of final volume) or medium (without FBS). Cholesterol efflux was calculated as follows: efflux= (MFI supernatant/ MFI cell lysate); % of efflux specific of the acceptor= (efflux with acceptor/efflux without acceptor)*100.

Reporter cells. 2B4–NFAT-GFP cells expressing *Clec4e* and/or FcR γ ⁸, were cultured in RPMI 1640 medium supplemented with 10% (vol/vol) FBS, and

stimulated (in RPMI 1640) with TDB (50 μ g/ml), PMA (500ng/ml; Sigma) or vehicle for 24 hours at 37°C. *Apoe*^{-/-} aortic extracts were obtained from 20 week female *Apoe*^{-/-} by cutting whole aorta in small pieces into complete medium. The resulting suspension was directly added to cells for 16 hours.

Statistical analysis. Values are expressed as means \pm s.e.m. Differences between values were examined using nonparametric Mann-Whitney (2 groups), Kruskal-Wallis followed by Dunn's test (\geq 2 groups) or two way ANOVA followed by Student T-test (Lesion density in aortic root) and were considered significant at $P < 0.05$.

Results

Clec4e senses necrosis in atherosclerotic arteries

To determine whether Clec4e can be activated by the necrotic core of atherosclerotic plaques, we took advantage of a NFAT-GFP reporter T cell line (originally Clec4e negative) transfected with the common FcR γ chain, with or without Clec4e. The presence of the reporter was confirmed by direct activation of NFAT by PMA, which induced GFP expression independently of Clec4e expression (Figure 1A). As expected, the synthetic Clec4e ligand (trehalose-6, 6'-dibehenate or TDB) ⁶ activated NFAT, inducing GFP expression only in cells expressing both Clec4e and Fc γ chain (Figure 1A). Importantly, activation of NFAT mediated GFP expression by atherosclerotic lysates from Apolipoprotein E

knockout (*ApoE*^{-/-}) mice was also *Clec4e* dependent, indicating that *Clec4e* signaling can be stimulated by plaque material (Figure 1B).

***Clec4e* is expressed in human and mouse atherosclerotic lesions**

We analyzed CLEC4E expression in human atherosclerotic lesions, and detected CLEC4E in myeloid cells (myeloperoxidase-positive, MPO⁺) infiltrating lesions, including intra-plaque MPO⁺ cells with foam cell morphology near the necrotic lipid core. Thus, CLEC4E is expressed in the vicinity of the necrotic core where it has the potential to sense necrosis (Figure 1C). In parallel, we found *Clec4e* expression on phagocytes (CD68⁺ cells) residing in the lipid core of advanced atherosclerotic lesions of *Ldlr*^{-/-} mice (Figure 1D).

***Clec4e* promotes atherosclerosis in *Ldlr*^{-/-} mice**

To address the role of *Clec4e* during atherogenesis *in vivo*, we performed a bone marrow (BM) transplantation experiment in *Ldlr*^{-/-} mice. Lethally-irradiated *Ldlr*^{-/-} mice were reconstituted with either *Clec4e*^{+/+} (*Clec4e*^{+/+} BM → *Ldlr*^{-/-}) or *Clec4e*^{-/-} (*Clec4e*^{-/-} BM → *Ldlr*^{-/-}) BM, and fed a high fat diet (HFD) for 20 weeks to induce advanced atherosclerotic lesions. Atherosclerosis was analyzed by Oil red O staining on the aortic sinus and the aortic arch. *Clec4e* deficiency in BM-derived cells led to a significant reduction in lesion development (30% to 35%) at both sites (Figures 1E and 1F), despite no change in the levels of plasma total cholesterol, HDL-cholesterol, triglycerides, and no change in animal weight (Figure I in the online-only Data Supplement). Closer inspection of Oil red O

staining revealed increased accumulation of neutral lipids in plaques of *Clec4e*^{+/+} BM → *Ldlr*^{-/-} mice as compared to *Clec4e*^{-/-} BM → *Ldlr*^{-/-} mice, suggesting a role for Clec4e in foam cell formation (Figure 1G).

Clec4e signaling enhances neutral lipid accumulation in macrophages

To understand how Clec4e might promote intracellular lipid accumulation, we determined whether Clec4e enhanced phagocytosis of oxLDL. Bone marrow-derived macrophages (BMDMs) from *Clec4e*^{+/+} and *Clec4e*^{-/-} mice were stimulated overnight with and without the synthetic Clec4e ligand, TDB, prior to incubation with Dil-oxLDL for 4 hours and analysis by flow cytometry. *Clec4e*^{+/+} and *Clec4e*^{-/-} BMDMs phagocytosed similar amounts of Dil-oxLDL, and pre-stimulation of Clec4e neither enhanced phagocytosis of Dil-oxLDL nor altered CD36 expression (Figure 2A). However, when we stained BMDMs and peritoneal macrophages (PEMs) incubated for 24 hours with unconjugated oxLDL using Bodipy 493/503 (a specific fluorescent dye for neutral lipids), we found WT cells accumulated more neutral lipids compared to *Clec4e*^{-/-} cells (Figure 2B and 2C). Furthermore, stimulation of Clec4e with TDB strongly enhanced lipid droplet accumulation in WT but not *Clec4e*^{-/-} macrophages (Figure 2B and 2C).

We speculated that the Clec4e induced accumulation of lipids could be due to a reduction in macrophage cholesterol efflux, because gene expression analysis revealed that TDB stimulation reduced the expression of both *Abca1* and *Abcg1* in WT but not *Clec4e*^{-/-} macrophages (Figure 2D). To test this hypothesis, we

loaded BMDMs of *Clec4e*^{+/+} and *Clec4e*^{-/-} mice with oxLDL for 24 hours in the presence or absence of TDB, and performed cholesterol efflux analysis using either mouse serum or the ApoA1-rich cholesterol acceptor, HDL. Compared to foam cells incubated with no acceptor, both mouse serum and human HDL increased the amount of fluorescent cholesterol released by 20% to 15%, respectively (Figure 2E). TDB significantly inhibited cholesterol release, and this was *Clec4e* dependent as no inhibition by TDB was observed in *Clec4e*^{-/-} macrophages (Figure 2E).

We investigated the role of *Clec4e* in cholesterol efflux further by flow cytometric analysis of *Abca1* expression, and found that TDB decreased oxLDL induced *Abca1* expression in PEMs (Figure 2F). To mimic the microenvironment of atherosclerotic plaques, we incubated macrophages with necrotic extracts of atherosclerotic *ApoE*^{-/-} aortas, containing both lipids and necrotic stimuli. We found that *Clec4e* expression in PEMs significantly prevented the up-regulation of *Abca1* in response to stimulation with plaque extracts (Figure 2G), indicating that *Clec4e* deficiency favors *Abca1* expression in a lipid-rich environment. Our data point to a new role for *Clec4e* in the development of macrophage-derived foam cells via inhibition of cholesterol efflux.

***Clec4e* induces an unfolded protein response (UPR) in macrophages**

Homeostasis of the endoplasmic reticulum (ER) is a tightly regulated process. Activation of the UPR upon ER stress aims to restore cellular homeostasis by

attenuating overall protein translation, degrading aberrant ER proteins and promoting expression of specific sets of genes to resolve the stress. However, if unresolved, ER-stress leads to cell death. During atherosclerosis, ER-stress in lesional macrophages^{15, 16} promotes the development of large necrotic cores via overactivation of the transcription factor CHOP and excessive induction of apoptosis. Since Clec4e signaling induces NFAT activation, which requires calcium efflux from ER stores, and leads to accumulation of neutral lipids in macrophages, we hypothesized that UPR-associated proteins may mediate, at least in part, Clec4e dependent effects in macrophages.

The lesions of *Clec4e*^{+/+} BM → *Ldlr*^{-/-} mice showed increased accumulation of MOMA-2⁺ foam cells (even when quantified per plaque surface area) compared to lesions of *Clec4e*^{-/-} BM → *Ldlr*^{-/-} mice (Figure 3A and 3B). Furthermore, we found a substantial reduction of both Syk phosphorylation (Figure 3A and 3B) and Chop expression (Figure 3C and 3D) in foam cells of *Clec4e*^{-/-} BM → *Ldlr*^{-/-} mice compared to mice transplanted with *Clec4e*^{+/+} BM. Interestingly, the number of apoptotic cells (Hoechst⁺TUNEL⁺) per section was similar between the two groups (data not shown). Therefore, we examined whether Clec4e signaling could directly activate the UPR in macrophages *in vitro*. We studied the induction of different markers specific to UPR/ER-stress at both the level of mRNA and protein. Whereas the basal level of expression of Clec4e was high in PEMs (Figure IIA in the online-only Data Supplement), the low basal level of Clec4e on BMDMs could be boosted by TDB stimulation in a Clec4e/Syk dependent

manner (Figure 3E, 3F and 3G). Stimulation of Clec4e/Syk by TDB induced Chop expression and Xbp1 mRNA splicing (sXbp1) (Figure 3E and 3F), suggesting the activation of several branches of the UPR. In turn, ER-stress induction by either thapsigargin or tunicamycin, promoted Clec4e expression in macrophages (Figure IIB in the online-only Data Supplement). Furthermore, Clec4e stimulation by TDB, like ER-stress induction by thapsigargin, induced an over-expression of Ire1 α protein and nuclear translocation of Chop in both BMDMs and PEMs (Figure 3H and 3I, and Figure IIC and IID in the online-only Data Supplement). We confirmed activation of Ire1 α RNA splicing activity (known to be responsible for Xbp1 splicing) after Clec4e stimulation using PEMs derived from the transgenic ER-stress-activated indicator (ERAI) mice (Figure 3J), which express the fluorescent Venus protein upon Ire1 α activation¹².

Clec4e signaling promotes a pro-inflammatory phenotype in macrophages through activation of the UPR

sXbp1 and Chop are integrated into innate and adaptive immune pathways, and affect cell fate and differentiation¹⁷. We found that lesions of *Clec4e*^{+/+} BM \rightarrow *Ldlr*^{-/-} mice had enhanced activation of innate and adaptive immune cells compared to lesions of *Clec4e*^{-/-} BM \rightarrow *Ldlr*^{-/-} mice. This was apparent through the significant increase in macrophages (Figure 3A) and T cells (Figure IIIA in the online-only Data Supplement) and the enhanced expression of inflammatory cytokines, e.g., Il1 β , by plaque foam cells of *Clec4e*^{+/+} BM \rightarrow *Ldlr*^{-/-} mice (Figure 4A). We also detected an increase in both CD8⁺ and CD4⁺ memory T cells

(CD44^{high}) in the spleen of *Clec4e*^{+/+} BM → *Ldlr*^{-/-} compared to *Clec4e*^{-/-} BM → *Ldlr*^{-/-} mice (Figure IIIB in the online-only Data Supplement), despite a similar distribution of immune cells between the 2 groups (Figure IIIC in the online-only Data Supplement). To examine the role of the ER stress in mediating inflammatory responses downstream of Clec4e, we studied BMDMs and PEMs derived from WT, *Chop*^{-/-} and *Ire1a*^{-/-} mice. Stimulation of Clec4e/Syk signaling by TDB induced the expression of several pro-inflammatory mediators (including Tnf- α and Ccl2) in BMDMs but reduced the expression of the anti-inflammatory cytokine TGF β (Figure IV in the online-only Data Supplement). This pro-inflammatory macrophage phenotype was reproduced in WT PEMs (Figure 4B), but was drastically prevented in *Chop*^{-/-} macrophages (Figure 4B). Intriguingly, Clec4e expression was partially controlled by Chop (Figure 4C), which may have contributed to the marked resistance of *Chop*^{-/-} macrophages to Clec4e stimulation. Chop deficiency also substantially reduced *sXbp1* expression in response to TDB and thapsigargin (Figure 4D), suggesting that Chop was activated upstream of *Ire1a*. Analysis of *Ire1a*^{-/-} PEMs by flow cytometry showed no difference in Clec4e expression compared to WT PEMs (Figure 4E), indicating that the control of Clec4e expression by Chop occurs upstream of *Ire1a* activation. Interestingly, *Ire1a*^{-/-} PEMs still showed a drastic reduction in Clec4e-dependent production of pro-inflammatory cytokines compared to WT PEMs (Figure 4F), despite no change in Clec4e expression. Furthermore, pharmacological inhibition of *Ire1a* splicing activity (STF inhibitor) in WT BMDMs recapitulated the *Ire1a* deficient phenotype (Figure VA and VB in the online-only

Data Supplement). These results reveal a crucial role for Chop and Ire1 α activation in the induction of a pro-inflammatory macrophage phenotype downstream of Clec4e, which may positively feed back to sustain Clec4e signaling through upregulation of Clec4e expression.

Clec4e/Chop/Ire1 α signaling promotes macrophage proliferation

When analyzing pro-inflammatory cytokine profile we found that the macrophage survival factor, Csf-1 was induced by TDB, and its expression was dependent on Ire1 α function (Figure VC in the online-only Data Supplement). This suggested a potential role for Clec4e signaling in macrophage survival or proliferation. We investigated this further by analyzing the expression of Ki67 in plaque macrophages. We found a significant reduction in the number of MOMA-2⁺ Ki67⁺ foam cells in *Clec4e*^{-/-} BM \rightarrow *Ldlr*^{-/-} compared to *Clec4e*^{+/+} BM \rightarrow *Ldlr*^{-/-} mice (Figure 5A). Furthermore, stimulation of macrophages with TDB *in vitro* promoted Ki67 expression, whereas thapsigargin-induced ER-stress promoted apoptosis (Figure 5B). TDB stimulation also reduced intra-nuclear levels of the cell cycle inhibitor p21^(WAF1/Cip1) (Figure 5C), along with a down-regulation of *Maf-b* and *c-Maf* but up-regulation of *Myc* and *Klf4* gene expression (Figure 5D), a phenotype previously shown to be crucial for macrophage self-renewal ¹⁸. TDB stimulated both macrophage proliferation and Csf1 expression in a Clec4e dependent manner (Figure 5E and 5F), and proliferation was significantly reduced by blockade of Csf1 production (Figure 5G). Finally, TDB-induced Csf1 expression (Figure 5H, and Figure V in the online-only Data Supplement) and proliferation

(Figure 5I) were markedly attenuated in the absence of Chop, or after inhibition of Ire1 α activity. Together, this data suggests Clec4e stimulation promotes macrophage proliferation, at least in part through induction of UPR/ER-stress-associated proteins.

Activating transcription factor 3 (Atf3) regulates Clec4e signaling in macrophages

Atf3, a member of the CREB family of basic leucine zipper transcription factors, is part of the UPR and has been shown to regulate both inflammatory and metabolic pathways^{19, 20}. Atf3 has an inhibitory role in atherosclerosis²¹; limiting macrophage foam cell formation by regulating intracellular neutral lipid accumulation through inhibition of cholesterol 25-hydroxylase²¹, and modulating cytokine production and ER stress²¹⁻²³. We hypothesized that if Atf3 is induced in response to Clec4e stimulation, it may limit macrophage foam cell formation and inflammation. Stimulation of macrophages with TDB induced nuclear translocation of Atf3 in a Clec4e dependent manner, in both PEMs and BMDMs (Figure 6A and 6B). Interestingly, Atf3 negatively regulated the acquisition of a pro-inflammatory phenotype by macrophages as shown by the significant increase of *Clec4e*, *Tnf* and *Ccl-2* expression in *Atf3*^{-/-} BMDMs incubated with TDB, compared to WT BMDMs (Figure 6C). Atf3 deficiency also promoted increased *Csf1* expression (Figure 6D) and enhanced proliferation (Figure 6E) in response to TDB, compared with WT macrophages. We found that oxLDL-induced *Abca1* expression was reduced in *Atf3*^{-/-} BMDMs, but Atf3 deficiency did

not alter TDB-dependent modulation of *Abca1* (Figure 6F). Thus implicating a negative feedback loop in which *Atf3* induced downstream of *Clec4e* limits *Clec4e*-dependent macrophage inflammation and proliferation, but not foam cell formation. Enhancement of the necrosis-*Clec4e* signaling axis could in part explain the acceleration of atherosclerosis in *Atf3*^{-/-} mice²¹.

Discussion

Previous studies reported activation of macrophage inflammatory responses downstream of *Clec4e*/*FcR γ* /*Syk*/*Card9*/*Nf- κ B* signaling²⁴. Here, we show that *Clec4e* stimulation induces a *Syk*-dependent ER stress-like response that directly contributes to *Clec4e*-dependent inflammatory responses. *Chop* and *Ire1 α* promote whereas *Atf3* limits and fine-tunes *Clec4e*-dependent atherogenic events.

The contribution of *Chop* to *Clec4e*-induced events is, at least in part, due to the upregulation of *Clec4e* expression. *Chop* binds and heterodimerizes with other members of the C/EBP family, most notably C/EBP β , and in doing so may inhibit or promote of C/EBP β transcriptional activity. Interaction between *Chop* and C/EBP β is required for nuclear localization of *Chop* and stabilization of C/EBP β ²⁵. In this regard, it is interesting to note that *Clec4e* was initially identified by virtue of its upregulation by LPS, which is mediated by C/EBP β ²⁶. C/EBP β has since been proposed to coordinate *Clec4e* expression and its downstream inflammatory gene induction²⁷. Therefore we speculate that *Chop*-dependent induction of *Clec4e* involves functional interaction between *Chop* and C/EBP β .

On the other hand, *Ire1a* deletion substantially inhibited Clec4e-induced inflammation without altering Clec4e expression. This is consistent with the role of *Ire1α* in promoting inflammatory responses via recruitment of Traf2 and activation of $\text{Nf-}\kappa\text{B}$ ²⁸ and Jnk²⁹ pathways, and/or via the production of sXbp1^{17, 30}.

Macrophage proliferation may contribute to atherosclerosis³¹. However, the mechanisms that orchestrate macrophage proliferation remain poorly defined. Here, Clec4e induced macrophage proliferation in a Chop- and *Ire1α*-mediated *Csf1* dependent manner, which is consistent with the major impact of *Csfr1* deletion on macrophage accumulation in atherosclerotic lesions³². Clec4e also induced a permissive state for macrophage proliferation through coordinated expression of transcription factors that are critical for self-renewal of differentiated macrophages; MafB, c-Maf, Klf4 and c-Myc¹⁸. Additional studies are needed to define the pathways linking Clec4e to these transcription factors. However, it is known that C/EBPβ isoform LIP plays a determinant role in repressing MafB³³, suggesting a similar role for Chop downstream of Clec4e signaling.

The role of Chop in atherosclerosis has mostly focused on induction of apoptotic cell death²³. Therefore, it is intriguing that Chop induction downstream of Clec4e did not promote apoptosis. The level of Chop induction by Clec4e is less pronounced compared to other inducers of ER stress, and therefore may not be sufficient to promote cell death. Furthermore, any pro-apoptotic effects of Chop may have been mitigated by the marked induction of *Csf1* downstream of

Clec4e, and the concomitant upregulation of sXbp1, another macrophage survival factor³⁴. A recent study reported a proliferative role for Chop in vascular smooth muscle cells (VSMCs), through downregulation of Klf4³⁵. Klf4 may either repress or enhance cell proliferation, dependent on cell sensitivity to p21^{Waf/Cip1}^{36, 37}. Reduced p21^{Waf/Cip1}, as observed in our Clec4e-stimulated macrophages, would favor a proliferative role of Klf4.

In agreement with previous reports linking ER stress to increased macrophage foam cell formation^{38, 39}, stimulation of Clec4e resulted in an ER stress-like response and concomitant induction of lipid body formation. The previous studies attributed the induction of foam cell formation to ER stress-induced upregulation of CD36 and/or Msr1, or to the promotion of an M2 macrophage phenotype^{38, 39}. Instead, our findings point to a role for Clec4e in the regulation of cholesterol efflux, in part through the inhibition of Abca1 expression. It is noteworthy that Chop represses *Pparγ*⁴⁰ and so might limit downstream *Abca1* transcription and Abca1-mediated cholesterol efflux⁴¹. Also of relevance here, Xbp1 activation triggers a triglyceride biosynthetic program in dendritic cells, which leads to lipid body formation⁴².

Additional work is needed to understand how Clec4e is engaged within atherosclerotic lesions. Clec4e signaling may be induced directly through recognition of necrotic cell death⁸, with or without concomitant (trans)activation of other pattern recognition receptors. Direct activation by other (yet unknown) ligands is also possible. In this regard, it is interesting to note that human, but not murine, CLEC4E binds cholesterol crystals, and mediates cholesterol-induced

pro-inflammatory responses in macrophages⁴³. This provides further support to the high relevance of our results to human atherogenesis.

The present study identified important roles for Clec4e in several aspects of macrophage function. However, additional studies will be needed to tease out the interactions between those biological pathways, particularly foam cell formation, proliferation and inflammatory status.

Finally, the study focused on the role of Clec4e in macrophages. Clec4e is not expressed on lymphocytes. However, other myeloid cells may contribute to Clec4e-dependent effects during atherosclerosis.

In conclusion, Clec4e plays a critical non-redundant role in promoting a pro-atherogenic macrophage phenotype, and aggravates atherosclerotic lesion inflammation. Our results support an important role for necrotic cell signaling in promoting the progression of advanced atherosclerotic plaques, and potential pathways for therapeutic intervention.

Acknowledgements

We gratefully acknowledge the assistance of the Department of Clinical Biochemistry, University of Cambridge for the analysis of serum biochemical parameters, and the Department of Medicine Phenotyping hub, University of Cambridge for assistance with flow cytometry.

Funding Sources

This work was supported by a European Research Council grant (to Z.M.), and by the British Heart Foundation (Z. M.).

Disclosures

None.

References

1. Tabas I, Garcia-Cardena G, Owens GK. Recent insights into the cellular biology of atherosclerosis. *J Cell Biol.* 2015;209:13-22
2. Russell DG, Cardona PJ, Kim MJ, Allain S, Altare F. Foamy macrophages and the progression of the human tuberculosis granuloma. *Nat Immunol.* 2009;10:943-948
3. Cambier CJ, Falkow S, Ramakrishnan L. Host evasion and exploitation schemes of Mycobacterium tuberculosis. *Cell.* 2014;159:1497-1509.
4. D'Avila H, Melo RC, Parreira GG, Werneck-Barroso E, Castro-Faria-Neto HC, Bozza PT. Mycobacterium bovis bacillus Calmette-Guerin induces TLR2-mediated formation of lipid bodies: intracellular domains for eicosanoid synthesis in vivo. *J Immunol.* 2006;176:3087-3097.
5. Bowdish DM, Sakamoto K, Kim MJ, Kroos M, Mukhopadhyay S, Leifer CA, Tryggvason K, Gordon S, Russell DG. MARCO, TLR2, and CD14 are required for macrophage cytokine responses to mycobacterial trehalose dimycolate and Mycobacterium tuberculosis. *PLoS Pathog.* 2009;5:e1000474.
6. Ishikawa E, Ishikawa T, Morita YS, Toyonaga K, Yamada H, Takeuchi O, Kinoshita T, Akira S, Yoshikai Y, Yamasaki S. Direct recognition of the mycobacterial glycolipid, trehalose dimycolate, by C-type lectin Mincle. *J Exp Med.* 2009;206:2879-2888.
7. Miyake Y, Masatsugu OH, Yamasaki S. C-Type Lectin Receptor MCL Facilitates Mincle Expression and Signaling through Complex Formation. *J Immunol.* 2015;194:5366-5374.

8. Yamasaki S, Ishikawa E, Sakuma M, Hara H, Ogata K, Saito T. Mincle is an ITAM-coupled activating receptor that senses damaged cells. *Nat Immunol.* 2008;9:1179-1188.
9. Hattori Y, Morita D, Fujiwara N, Mori D, Nakamura T, Harashima H, Yamasaki S, Sugita M. Glycerol monomycolate is a novel ligand for the human, but not mouse macrophage inducible C-type lectin, Mincle. *J Biol Chem.* 2014;289:15405-15412.
10. Yamasaki S, Matsumoto M, Takeuchi O, Matsuzawa T, Ishikawa E, Sakuma M, Tateno H, Uno J, Hirabayashi J, Mikami Y, Takeda K, Akira S, Saito T. C-type lectin Mincle is an activating receptor for pathogenic fungus, *Malassezia*. *Proc Natl Acad Sci U S A.* 2009;106:1897-1902.
11. Iwawaki T, Akai R, Yamanaka S, Kohno K. Function of IRE1 alpha in the placenta is essential for placental development and embryonic viability. *Proc Natl Acad Sci U S A.* 2009;106:16657-16662.
12. Iwawaki T, Akai R, Kohno K, Miura M. A transgenic mouse model for monitoring endoplasmic reticulum stress. *Nat Med.* 2004;10:98-102.
13. Hartman MG, Lu D, Kim ML, Kociba GJ, Shukri T, Buteau J, Wang X, Frankel WL, Guttridge D, Prentki M, Grey ST, Ron D, Hai T. Role for activating transcription factor 3 in stress-induced beta-cell apoptosis. *Mol Cell Biol.* 2004;24:5721-5732.
14. Taleb S, Herbin O, Ait-Oufella H, Verreth W, Gourdy P, Barateau V, Merval R, Esposito B, Clement K, Holvoet P, Tedgui A, Mallat Z. Defective Leptin/Leptin Receptor Signaling Improves Regulatory T Cell Immune Response and Protects Mice From Atherosclerosis. *Arterioscler Thromb Vasc Biol.* 2007; 27:2691-2698.

15. Feng B, Yao PM, Li Y, Devlin CM, Zhang D, Harding HP, Sweeney M, Rong JX, Kuriakose G, Fisher EA, Marks AR, Ron D, Tabas I. The endoplasmic reticulum is the site of cholesterol-induced cytotoxicity in macrophages. *Nat Cell Biol.* 2003;5:781-792.
16. Myoishi M, Hao H, Minamino T, Watanabe K, Nishihira K, Hatakeyama K, Asada Y, Okada K, Ishibashi-Ueda H, Gabbiani G, Bochaton-Piallat ML, Mochizuki N, Kitakaze M. Increased endoplasmic reticulum stress in atherosclerotic plaques associated with acute coronary syndrome. *Circulation.* 2007;116:1226-1233.
17. Bettigole SE, Glimcher LH. Endoplasmic reticulum stress in immunity. *Annu Rev Immunol.* 2015;33:107-138.
18. Aziz A, Soucie E, Sarrazin S, Sieweke MH. MafB/c-Maf deficiency enables self-renewal of differentiated functional macrophages. *Science.* 2009;326:867-871.
19. Gilchrist M, Thorsson V, Li B, Rust AG, Korb M, Roach JC, Kennedy K, Hai T, Bolouri H, Aderem A. Systems biology approaches identify ATF3 as a negative regulator of Toll-like receptor 4. *Nature.* 2006;441:173-178.
20. De Nardo D, Labzin LI, Kono H, Seki R, Schmidt SV, Beyer M, Xu D, Zimmer S, Lahrmann C, Schildberg FA, Vogelhuber J, Kraut M, Ulas T, Kerksiek A, Krebs W, Bode N, Grebe A, Fitzgerald ML, Hernandez NJ, Williams BR, Knolle P, Kneilling M, Rocken M, Lutjohann D, Wright SD, Schultze JL, Latz E. High-density lipoprotein mediates anti-inflammatory reprogramming of macrophages via the transcriptional regulator ATF3. *Nat Immunol.* 2014;15:152-160.

21. Gold ES, Ramsey SA, Sartain MJ, Selinummi J, Podolsky I, Rodriguez DJ, Moritz RL, Aderem A. ATF3 protects against atherosclerosis by suppressing 25-hydroxycholesterol-induced lipid body formation. *J Exp Med*. 2012;209:807-817.
22. Hai T, Wolford CC, Chang YS. ATF3, a hub of the cellular adaptive-response network, in the pathogenesis of diseases: is modulation of inflammation a unifying component? *Gene Expr*. 2010;15:1-11.
23. Seimon TA, Kim MJ, Blumenthal A, Koo J, Ehrt S, Wainwright H, Bekker LG, Kaplan G, Nathan C, Tabas I, Russell DG. Induction of ER stress in macrophages of tuberculosis granulomas. *PLoS One*. 2010;5:e12772.
24. Sancho D, Reis e Sousa C. Sensing of cell death by myeloid C-type lectin receptors. *Curr Opin Immunol*. 2013;25:46-52.
25. Chiribau CB, Gaccioli F, Huang CC, Yuan CL, Hatzoglou M. Molecular symbiosis of CHOP and C/EBP beta isoform LIP contributes to endoplasmic reticulum stress-induced apoptosis. *Mol Cell Biol*. 2010;30:3722-3731.
26. Matsumoto M, Tanaka T, Kaisho T, Sanjo H, Copeland NG, Gilbert DJ, Jenkins NA, Akira S. A novel LPS-inducible C-type lectin is a transcriptional target of NF-IL6 in macrophages. *J Immunol*. 1999;163:5039-5048.
27. Schoenen H, Huber A, Sonda N, Zimmermann S, Jantsch J, Lepenies B, Bronte V, Lang R. Differential control of Mincle-dependent cord factor recognition and macrophage responses by the transcription factors C/EBPbeta and HIF1alpha. *J Immunol*. 2014;193:3664-3675.
28. Hu P, Han Z, Couvillon AD, Kaufman RJ, Exton JH. Autocrine tumor necrosis factor alpha links endoplasmic reticulum stress to the membrane

death receptor pathway through IRE1 α -mediated NF- κ B activation and down-regulation of TRAF2 expression. *Mol Cell Biol.* 2006;26:3071-3084.

29. Urano F, Wang X, Bertolotti A, Zhang Y, Chung P, Harding HP, Ron D. Coupling of stress in the ER to activation of JNK protein kinases by transmembrane protein kinase IRE1. *Science.* 2000;287:664-666.

30. Martinon F, Chen X, Lee AH, Glimcher LH. TLR activation of the transcription factor XBP1 regulates innate immune responses in macrophages. *Nat Immunol.* 2010;11:411-418.

31. Robbins CS, Hilgendorf I, Weber GF, Theurl I, Iwamoto Y, Figueiredo JL, Gorbato R, Sukhova GK, Gerhardt LM, Smyth D, Zavitz CC, Shikatani EA, Parsons M, van Rooijen N, Lin HY, Husain M, Libby P, Nahrendorf M, Weissleder R, Swirski FK. Local proliferation dominates lesional macrophage accumulation in atherosclerosis. *Nat Med.* 2013;19:1166-1172.

32. Smith JD, Trogan E, Ginsberg M, Grigaux C, Tian J, Miyata M. Decreased atherosclerosis in mice deficient in both macrophage colony-stimulating factor (op) and apolipoprotein e. *Proc Natl Acad Sci USA.* 1995;92:8264-8268.

33. Smink JJ, Begay V, Schoenmaker T, Sterneck E, de Vries TJ, Leutz A. Transcription factor C/EBP β isoform ratio regulates osteoclastogenesis through MafB. *EMBO J.* 2009;28:1769-1781.

34. Tian PG, Jiang ZX, Li JH, Zhou Z, Zhang QH. Spliced XBP1 promotes macrophage survival and autophagy by interacting with Beclin-1. *Biochem Biophys Res Commun.* 2015;463:518-523.

35. Zhou AX, Wang X, Lin CS, Han J, Yong J, Nadolski MJ, Boren J, Kaufman RJ, Tabas I. C/EBP-Homologous Protein (CHOP) in Vascular

Smooth Muscle Cells Regulates Their Proliferation in Aortic Explants and Atherosclerotic Lesions. *Circ Res*. 2015;116:1736-1743.

36. Yoshida T, Kaestner KH, Owens GK. Conditional deletion of Kruppel-like factor 4 delays downregulation of smooth muscle cell differentiation markers but accelerates neointimal formation following vascular injury. *Circ Res*. 2008;102:1548-1557
37. Rowland BD, Peeper DS. KLF4, p21 and context-dependent opposing forces in cancer. *Nat Rev Cancer*. 2006;6:11-23.
38. Oh J, Riek AE, Weng S, Petty M, Kim D, Colonna M, Cella M, Bernal-Mizrachi C. Endoplasmic reticulum stress controls M2 macrophage differentiation and foam cell formation. *J Biol Chem*. 2012;287:11629-11641.
39. Yao S, Miao C, Tian H, Sang H, Yang N, Jiao P, Han J, Zong C, Qin S. Endoplasmic reticulum stress promotes macrophage-derived foam cell formation by up-regulating cluster of differentiation 36 (CD36) expression. *J Biol Chem*. 2014;289:4032-4042.
40. Park SH, Choi HJ, Yang H, Do KH, Kim J, Lee DW, Moon Y. Endoplasmic reticulum stress-activated C/EBP homologous protein enhances nuclear factor-kappaB signals via repression of peroxisome proliferator-activated receptor gamma. *J Biol Chem*. 2010;285:35330-35339.
41. Chinetti G, Lestavel S, Bocher V, Remaley AT, Neve B, Torra IP, Teissier E, Minnich A, Jaye M, Duverger N, Brewer HB, Fruchart JC, Clavey V, Staels B. PPAR-alpha and PPAR-gamma activators induce cholesterol removal from human macrophage foam cells through stimulation of the ABCA1 pathway. *Nat Med*. 2001;7:53-58.

42. Cubillos-Ruiz JR, Silberman PC, Rutkowski MR, Chopra S, Perales-Puchalt A, Song M, Zhang S, Bettigole SE, Gupta D, Holcomb K, Ellenson LH, Caputo T, Lee AH, Conejo-Garcia JR, Glimcher LH. ER Stress Sensor XBP1 Controls Anti-tumor Immunity by Disrupting Dendritic Cell Homeostasis. *Cell*. 2015;161:1527-1538.
43. Kiyotake R, Oh-Hora M, Ishikawa E, Miyamoto T, Ishibashi T, Yamasaki S. Human Mincle Binds to Cholesterol Crystals and Triggers Innate Immune Responses. *J Biol Chem*. 2015;290:25322-25332.

Figure legends

Figure 1. Clec4e senses necrotic debris and promotes atherosclerosis.

A,B- Flow cytometry analysis of GFP expression by 2B4–NFAT-GFP cells transfected with Clec4e and/or FcR γ expression plasmids, then treated for 24 hours with PMA, TDB or vehicle alone (A), or with aortic extract from *ApoE*^{-/-} mice (B). Data were obtained using technical quadruplicates, and are representative of at least 2 independent experiments. (*p<0.05, **p<0.01: FcR γ vs FcR γ + Clec4e in the same condition, Kruskal-Wallis & Dunn post test). C- Expression of CLEC4E protein by myeloid cells in human atherosclerotic coronary artery. Top left panel: overview of an atherosclerotic plaque using Masson's trichrome. Top right panel: distribution of myeloid cells (MPO⁺) within the atherosclerotic lesion analyzed by fluorescence microscopy (Top panel's scale bars: 300 μ m). Bottom panels: CLEC4E expression by media infiltrating myeloid cells (left panel) and foam cells near the necrotic/lipid core of the plaque (right panel) analyzed by confocal microscopy (Bottom panel's scale bars: 20 μ m). D- Confocal analysis of Clec4e expression by phagocytes (CD68⁺) in atherosclerotic lesions of *Ldlr*^{-/-} after BM transfer and 20 weeks of HFD. Images are representative of 3 mice (Scale bar: 50 μ m). E, F- Analysis of atherosclerosis development in *Ldlr*^{-/-} mice engrafted with *Clec4e*^{+/+} or *Clec4e*^{-/-} BM and kept under HFD for 20 weeks (n=8 mice/group). Representative Oil red O' stainings of aortic root cross sections (E) and of "en face" aortic arch (F) with histograms depicting atherosclerosis lesion density (% of vessel area) (Scale bar: 500 μ m). G- Representative images of Oil red O stainings in plaques of *Clec4e*^{+/+} BM -> *Ldlr*^{-/-} and *Clec4e*^{-/-} BM -> *Ldlr*^{-/-} (Scale bar: 100 μ m) with histograms depicting Oil red O density

(% of plaque area). * $p < 0.05$, ** $p < 0.01$, 2-way ANOVA (E) and Mann-Whitney test (F, G).

Figure 2. Clec4e enhances neutral lipid accumulation in macrophages, through inhibition of cholesterol efflux. A- Flow cytometry analysis of Dil-oxLDL uptake (4 hours) by BMDMs from *Clec4e*^{+/+} and *Clec4e*^{-/-}, with or without pre-conditioning with TDB, and CD36 expression by BMDMs in the same conditions. B, C- Flow cytometry analysis of Bodipy 493/503 staining on BMDMs (B) and PEMs (C) from *Clec4e*^{+/+} and *Clec4e*^{-/-} incubated in the presence, or not, of oxLDL, with or without TDB for 24 hours. *p<0.05 *Clec4e*^{+/+} vs *Clec4e*^{-/-} oxLDL + TDB-treated cells. D- RT/Q-PCR analysis of *Abca1* and *Abcg1* mRNA expression by *Clec4e*^{+/+} and *Clec4e*^{-/-} BMDMs treated with or without TDB. *p<0.05, TDB- vs vehicle-treated BMDMs. E- Cholesterol efflux analysis of *Clec4e*^{+/+} and *Clec4e*^{-/-} BMDMs stimulated for 24 hours with oxLDL ± TDB, using fluorescently labelled cholesterol. The efflux of cholesterol was induced by the addition of mouse serum or human purified HDLs in the medium for 4h. *p<0.05 TDB- vs vehicle-treated BMDMs + oxLDL. F- Flow cytometry analysis of *Abca1* expression on PEMs stimulated with oxLDL (black line), oxLDL with TDB (bleu line). Grey line represents unstained cells. G- Flow cytometry analysis of *Abca1* expression by PEMs from *Clec4e*^{+/+} and *Clec4e*^{-/-} mice stimulated necrotic aortic extract from *ApoE*^{-/-} mice for 24 hours. *p<0.05 *ApoE*^{-/-} necrotic aorta vs vehicle-treated *Clec4e*^{+/+} PEMs; *p<0.05 *ApoE*^{-/-} necrotic aorta vs vehicle-treated *Clec4e*^{-/-} PEMs; #p<0.05 *Clec4e*^{-/-} vs *Clec4e*^{+/+} vehicle-treated PEMs. Data were obtained using technical quadruplicates, and are representative of at least 2 independent experiments. Kruskal-Wallis with Dunn's test (B-E, G).

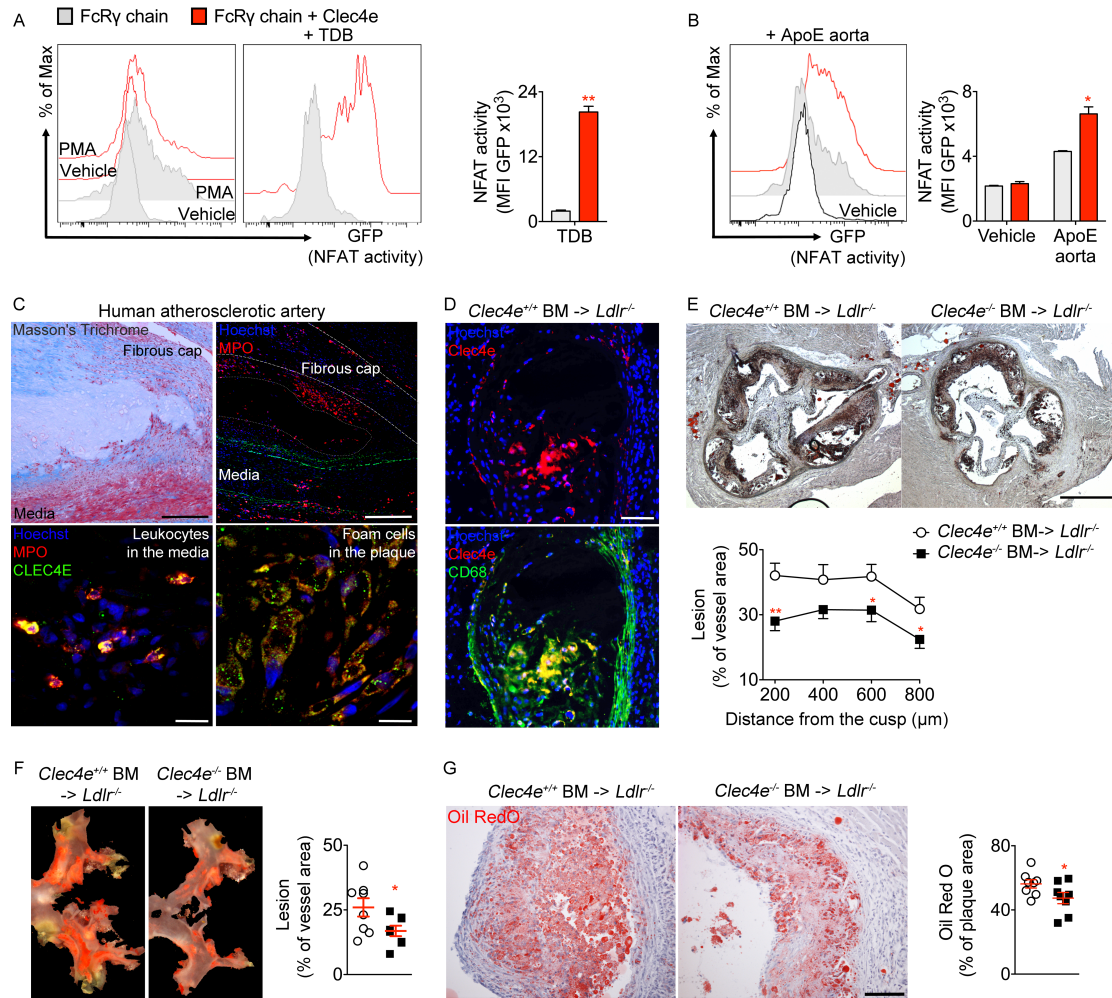
Figure 3. Stimulation of the Clec4e/Syk axis induces UPR in macrophages. A, B- Epifluorescence analysis of the expression of the foam cell-associated epitope MOMA-2 and phospho-Syk Y323 (pSyk) on aortic root cross-sections (n= 8 mice/group). Representative images of MOMA-2 and pSyk stainings in lesions of *Clec4e*^{+/+} BM → *Ldlr*^{-/-} and *Clec4e*^{-/-} BM → *Ldlr*^{-/-} mice (A) and quantification of MOMA-2⁺ area and co-stained MOMA-2/pSyk area (B) (Scale bar: 250μm). C, D- Epifluorescence analysis of the expression of Chop by MOMA-2⁺ cells on aortic root cross sections of *Clec4e*^{+/+} BM → *Ldlr*^{-/-} and *Clec4e*^{-/-} BM → *Ldlr*^{-/-} mice (n= 8 mice/group). Quantification of Chop MFI in MOMA-2⁺ area (C) and representative images of MOMA-2 and Chop stainings in lesions (D) (Scale bar: 150μm). E, F- RT/Q-PCR analysis of *Clec4e*, *sXbp1* and *Chop* expression by *Clec4e*^{+/+} and *Clec4e*^{-/-} BMDMs (E) or BMDMs with or without Syk inhibitor (Syk inh; R406) (F) stimulated with TDB for 12 hours. *p<0.05 TDB- vs vehicle-treated *Clec4e*^{+/+} BMDMs vs all other conditions. G, H, I- *Clec4e*, *Ire1a* and *Chop* protein expression by BMDMs treated with TDB or thapsigargin for 16 hours analyzed by confocal microscopy (Scale bar: 50μm). (n= 30-50 cells/conditions; *p<0.05, ***p<0.001 TDB- or thapsigargin- vs vehicle-treated BMDMs; Scale bar: 20μm). J- Flow cytometry analysis of Venus-FP expression by WT or ERAI PEMs incubated in the presence the vehicle alone, or TDB for 24 hours. Data were obtained using technical quadruplicates, and are representative of 4 independent experiments. Mann-Whitney (B, C) and Kruskal-Wallis with Dunn's test (E, F, H, I).

Figure 4. Clec4e-induced UPR activation stimulates pro-inflammatory cytokine production by macrophages, via Chop and Ire1 α . A- Epifluorescence analysis of the expression of Il-1 β by MOMA-2⁺ cells on cross section of *Clec4e*^{+/+} BM \rightarrow *Ldlr*^{-/-} and *Clec4e*^{-/-} BM \rightarrow *Ldlr*^{-/-} mice. Representative images of MOMA-2 and Il-1 β stainings in lesions and quantification of Il-1 β MFI in MOMA-2⁺ area (Scale bar: 150 μ m). B- Pro-inflammatory cytokine (Tnf- α , Il-6 and Il-1 β) secretion by *Clec4e*^{+/+}, *Clec4e*^{-/-} and *Chop*^{-/-} PEMs stimulated with TDB for 16 hours. *p<0.05 TDB-stimulated *Clec4e*^{+/+} BMDMs vs all conditions. C- Flow cytometry analysis of Clec4e expression on PEMs from *Clec4e*^{+/+}, *Clec4e*^{-/-} and *Chop*^{-/-} mice. Dotted line on the histogram represents Clec4e staining on *Clec4e*^{-/-} PEMs. *p<0.05 *Clec4e*^{+/+} vs *Chop*^{-/-} PEMs. D- RT/Q-PCR analysis of *Clec4e* and *sXbp1* by *Chop*^{+/+} and *Chop*^{-/-} BMDMs treated with TDB or thapsigargin for 12 hours. *p<0.05, *Chop*^{+/+} vs *Chop*^{-/-} BMDMs from the same condition. E- Flow cytometry analysis of Clec4e expression on PEMs from *Ire1a*^{+/+} (*LysM-Cre*⁻ *Ire1a*^{flox/flox}) and *Ire1a*^{-/-} (*LysM-Cre*⁺ *Ire1a*^{flox/flox}) mice. F- Cytokine (Tnf- α , Il-6, Il-1 β , Il-1 α , Ccl-2 and Il-10) secretion by *Ire1a*^{+/+} and *Ire1a*^{-/-} PEMs stimulated with TDB for 16 hours. *p<0.05 TDB- vs Vehicle stimulated *Ire1a*^{+/+} BMDMs. Data were obtained using technical quadruplicates, and are representative of at least 2 independent experiments. Mann-Whitney (A, C) and Kruskal-Wallis with Dunn's test (B, D, F).

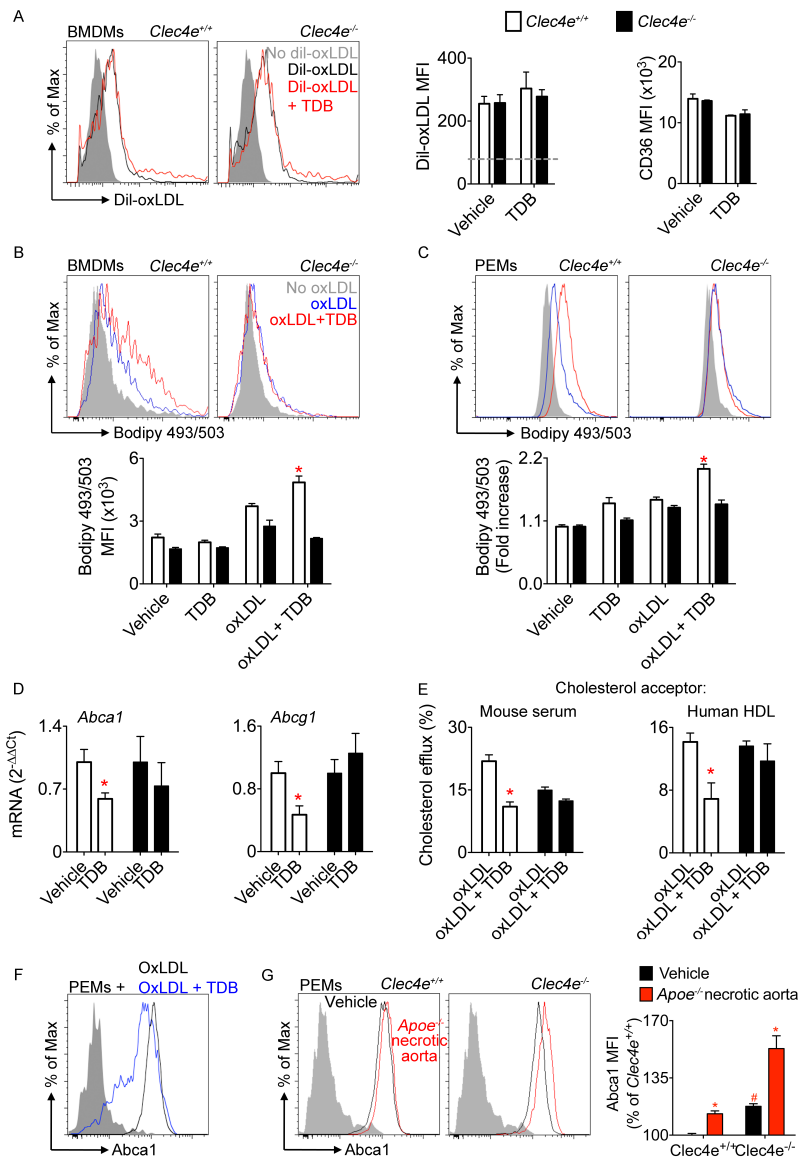
Figure 5. Clec4e induces proliferation of macrophages via a Csf1-autocrine loop regulated by Chop and Ire1 α . A- Epifluorescence analysis of the expression of Ki67 by MOMA-2⁺ area on aortic cross sections of *Clec4e*^{+/+} BM \rightarrow *Ldlr*^{-/-} and *Clec4e*^{-/-} BM \rightarrow *Ldlr*^{-/-} mice (n= 8 mice/group). Representative images of MOMA-2 and Ki67 stainings in lesions and quantification of MOMA-2⁺Ki67⁺ cells per sections (Scale bar: 25 μ m). *p<0.05, Mann-Whitney test. B- Ki67 protein expression by BMDMs treated with vehicle, TDB or thapsigargin (12 hours) and TUNEL stainings analyzed by confocal microscopy (Scale bar: 50 μ m). C- p21^(Waf1/Cip1) protein expression by BMDMs treated with, or without, TDB for 12 hours and analyzed by confocal microscopy (Scale bar: 20 μ m). *p<0.05, Student t test (n=30-50 cells/group). D- RT/Q-PCR analysis of *Klf4*, *Myc*, *cMaf* and *Maf-b* mRNA expression by BMDMs treated with or without TDB for 12 hours. *p<0.05, TDB- vs vehicle-treated BMDMs, Mann-Whitney test. E- Cell number estimation experiment using MTT assay. The percentage of proliferation is expressed as = (MTT O.D. sample * 100 / MTT O.D. vehicle)-100. *Clec4e*^{+/+} and *Clec4e*^{-/-} BMDMs were stimulated for 24 hours with TDB. *p<0.05, TDB- vs vehicle-treated BMDMs. F- ELISA titration of Csf1 secretion by PEMs from *Clec4e*^{+/+} and *Clec4e*^{-/-} mice stimulated with TDB for 24 hours. *p<0.05, *Clec4e*^{+/+} vs *Clec4e*^{-/-} TDB-treated PEMs. G- TDB induced BMDMs proliferation can be abrogated by the addition of an anti-Csf1 antibody in the culture medium **p<0.01, Isotype vs anti-Csf1 treated BMDMs, 2-way ANOVA test. H- RT/Q-PCR analysis of *Csf1* mRNA expression by BMDMs (*Clec4e*^{+/+}, *Chop*^{-/-} or *Clec4e*^{-/-}) treated with or without TDB for 16 hours. *p<0.05, TDB- vs vehicle-treated BMDMs from the same genotype. I- TDB induced BMDMs proliferation

requires Chop and Ire1a expression. * $p < 0.05$, TDB- vs vehicle-treated WT BMDMs. Data were obtained using technical quadruplicates, and are representative of at least 2 independent experiments. Kruskal-Wallis with Dunn's test (E, F, H, I).

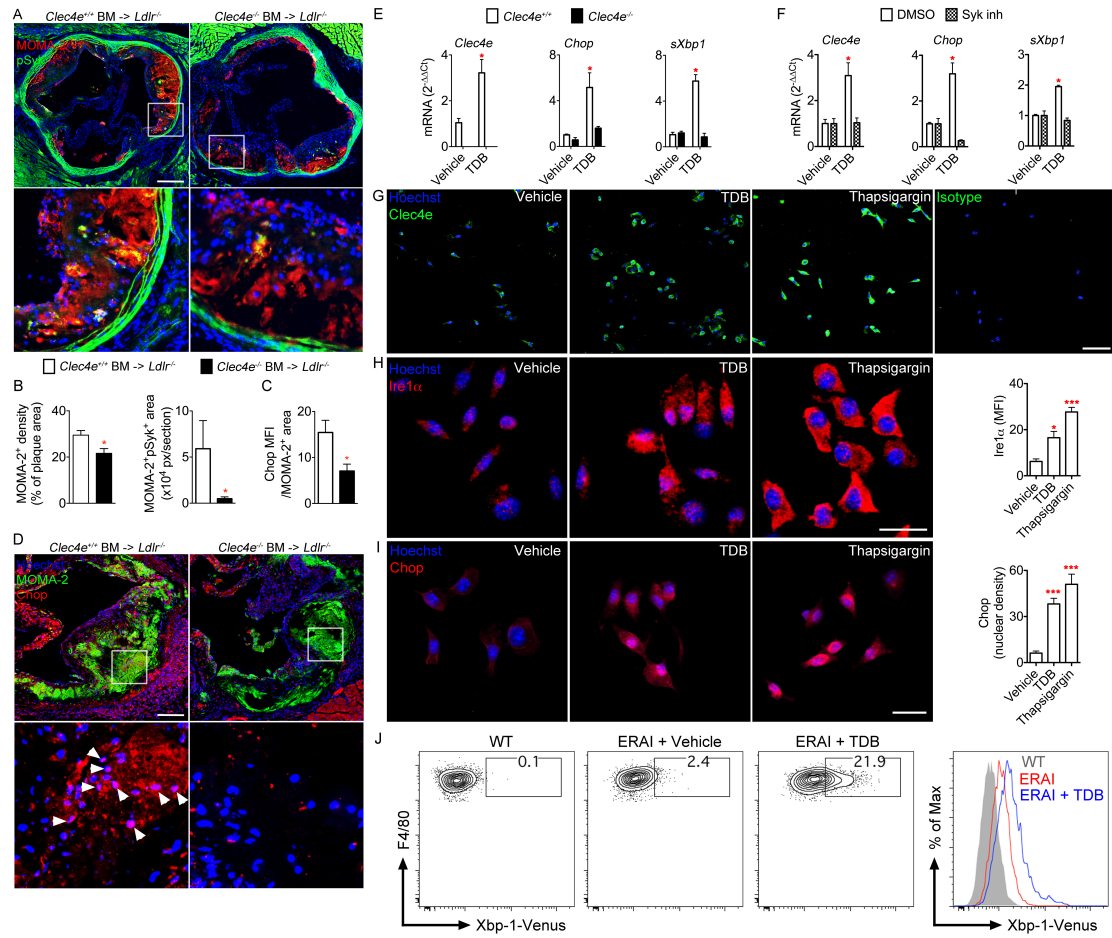
Figure 6. Atf3 modulates Clec4e signaling pathway in macrophages. A, B- Atf3 protein expression, and nuclear translocation, by BMDMs (A, Scale bar: 20 μ m) and PEMs (B, Scale bar: 10 μ m) treated for 16 hours with vehicle, TDB or thapsigargin, , analyzed by confocal microscopy. ** $p < 0.01$, *** $p < 0.001$ TDB- or thapsigargin- vs vehicle-treated BMDMs A, B: 20-30 cells analyzed/condition, data are representative of 3 independent experiments. C, D, E- RT/Q-PCR analysis of *Clec4e*, *Tnf- α* , *Ccl-2* (C), and *Csf1* (D) mRNA expression by *Atf3*^{+/+} and *Atf3*^{-/-} BMDMs treated with or without TDB for 12 hours. * $p < 0.05$, *Atf3*^{-/-} vs *Atf3*^{+/+} TDB-treated BMDMs. E- Percentage of proliferation of TDB-stimulated *Atf3*^{-/-} BMDMs over TDB-stimulated *Atf3*^{+/+} BMDMs assessed by MTT after 36h of stimulation (* $p < 0.05$ *Atf3*^{-/-} vs *Atf3*^{+/+}). F- RT/Q-PCR analysis of *Abca1* mRNA expression by *Atf3*^{+/+} and *Atf3*^{-/-} BMDMs treated with or without oxLDL and TDB for 12 hours. * $p < 0.05$, oxLDL- and oxLDL + TDB-treated *Atf3*^{+/+} BMDMs. C-F: Data were obtained using technical quadruplicates, and are representative of 2 independent experiments. Mann-Whitney (E) and Kruskal-Wallis with Dunn's test (A, C, D, F).



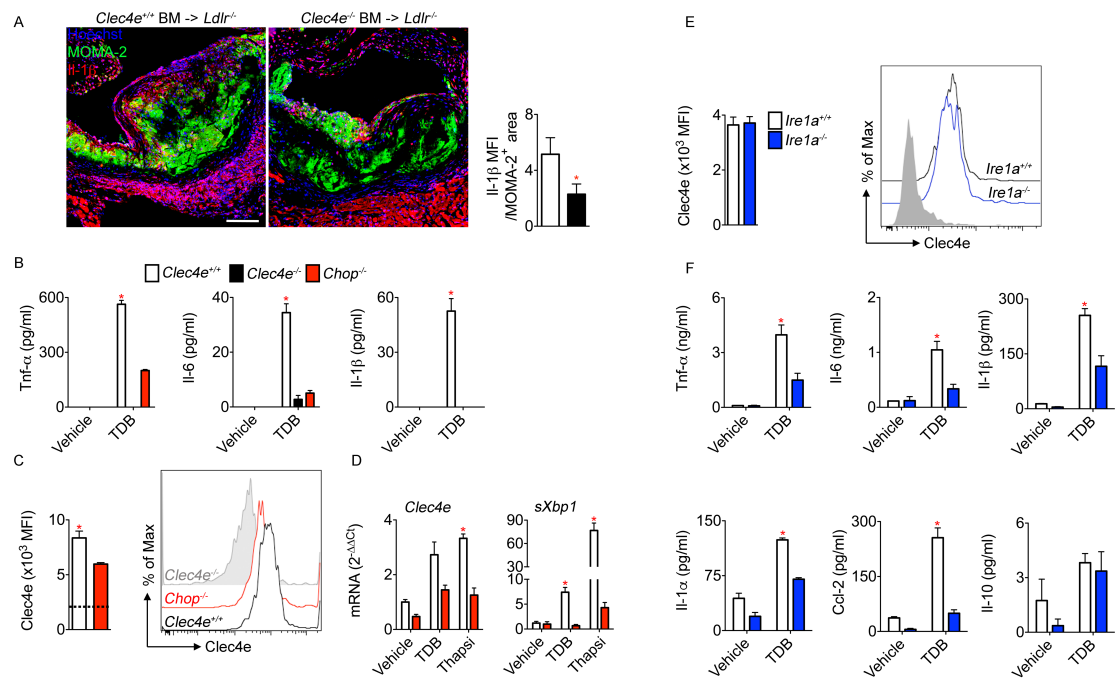
Clément, Necrotic sensor Clec4e promotes atherosclerosis



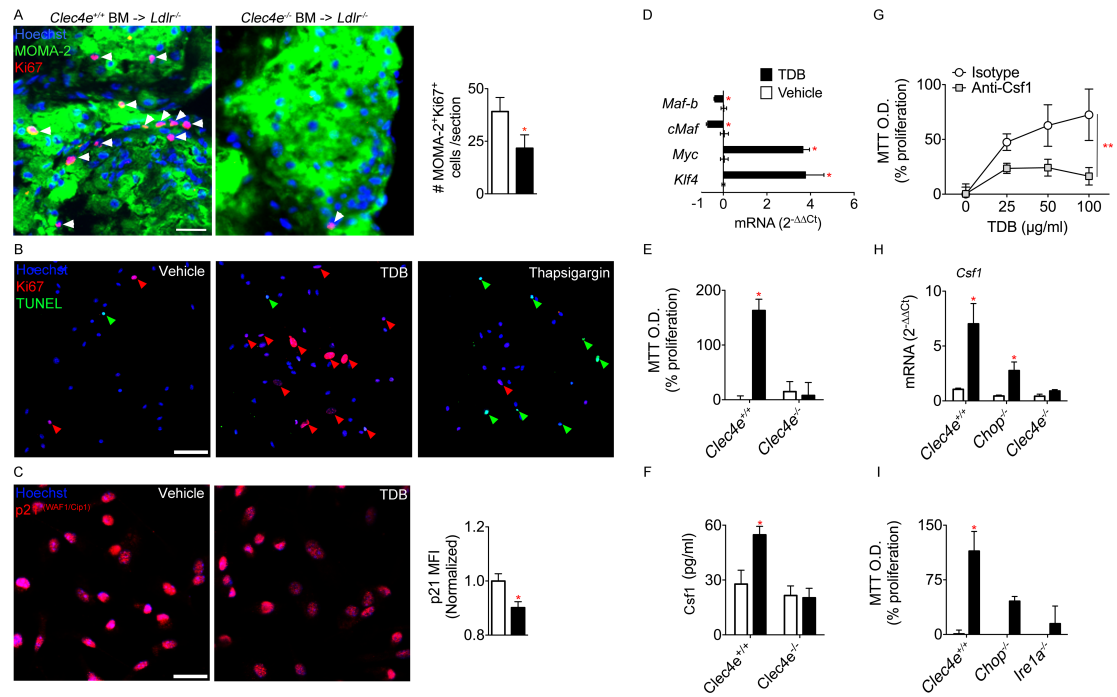
Clément, Necrotic sensor Clec4e promotes atherosclerosis



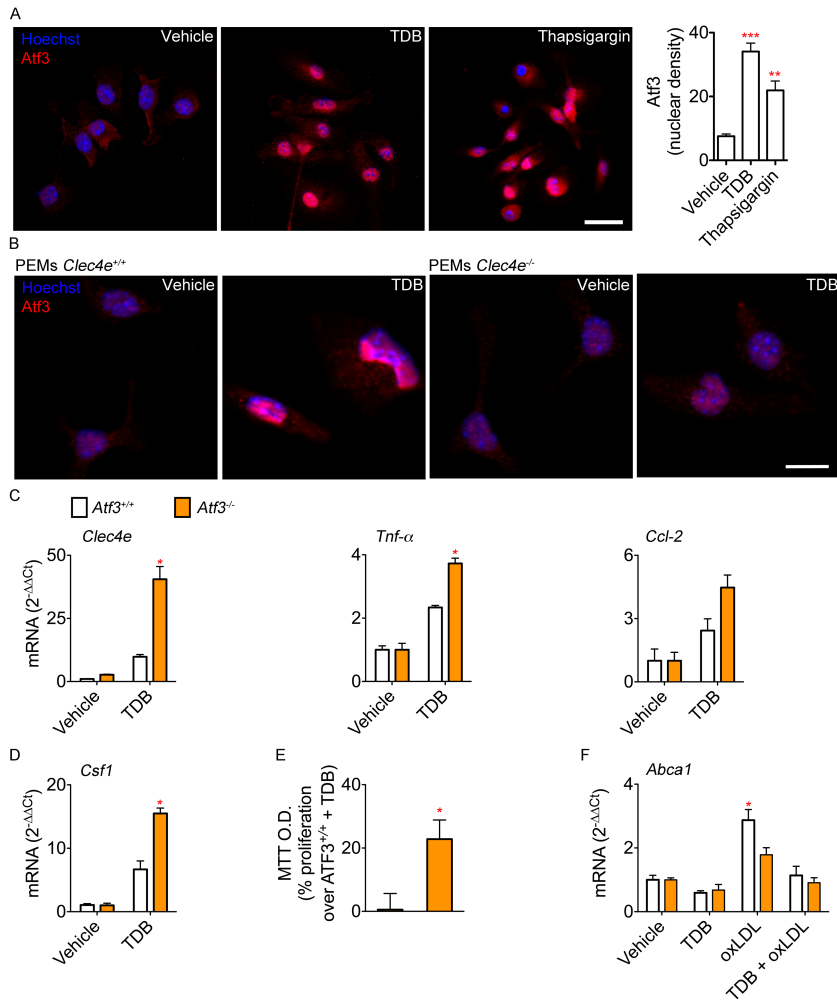
Clément, Necrotic sensor Clec4e promotes atherosclerosis



Clément, Necrotic sensor Clec4e promotes atherosclerosis



Clément, Necrotic sensor Clec4e promotes atherosclerosis



Clément, Necrotic sensor Clec4e promotes atherosclerosis

Clément, Necrotic sensor Clec4e promotes atherosclerosis

SUPPLEMENTAL MATERIAL

Supplemental Methods

Animals. Animal experiments were approved by the Home Office, UK, and were performed under PPL 80/2426. All mice were on C57Bl/6 background. *Clec4e*^{-/-} 1, *Chop*^{-/-} (Jackson laboratories), *Ire1a*^{flox/flox} 2, ERAI 3 and *Atf3*^{-/-} 4 mice were previously described. Male 6-8 week old *Ldlr*^{-/-} mice were lethally irradiated (9.5 Gy) then injected i.v. with 1x10⁷ bone marrow cells from donor mice. After 4 weeks recovery, mice were fed a high fat diet (21 % Fat, 0.15 % Cholesterol, Special Diet Services) for 20 weeks. Littermate *Clec4e*^{+/+}, *Clec4e*^{-/-} mice were used as donors for bone marrow transfer to *Ldlr*^{-/-} animals. Aorta were removed, fixed (PFA 4%, 16 hours at 4°C) and kept in PBS for further investigations.

Bone marrow-derived macrophages (BMDMs) and peritoneal macrophages (PEMs) were derived from age- and sex-matched mice (*Clec4e*^{+/+}, *Clec4e*^{-/-}, *Chop*^{+/+}, *Chop*^{-/-}, *LysM-Cre*⁺ *Ire1a*^{flox/flox}, *LySM-Cre*⁻ *Ire1a*^{flox/flox}, *Atf3*^{+/+}, *Atf3*^{-/-}; n=3-4/groups).

Cholesterol analysis. Blood was obtained by cardiac puncture on EDTA. Plasma and cells were separated by centrifugation (15 minutes 15,000 g). Plasma was kept at -80°C for cholesterol analysis and cells were used to look at myeloid cell distribution. Triglycerides, total cholesterol and HDL were quantified on plasma (EDTA) by the Core Biochemical Assay lab at the University of Cambridge.

Cell culture. Cells were cultured at 37°C and in 5 % CO₂ in a humidified incubator. Primary mouse BMDMs were prepared using femoral BM cells (2×10^6 cell/10 ml/petri dish) in BMDM medium (RPMI 1640 containing L-glutamine + 10 % [vol/vol] heat-inactivated FBS, 100 IU/ml penicillin, 100 µg/ml streptomycin and 30 % L929 medium). On day 4, 10 ml of fresh BMDM medium was added, and on day 8, adherent cells were lifted using ice-cold PBS, counted, pelleted, resuspended in complete medium, and used for stimulation at a cell density of 5×10^5 cell/well in 24-well plates.

PEMs were obtained by injecting 5 ml of ice-cold PBS i.p. in mice. Peritoneal exudates were pelleted, resuspended in complete RPMI, and plated in 24-well plates at a density of 1×10^6 cells/well. Non-adhering cells were harvested 4 hours after plating and the remaining PEMs were used for stimulation (>95 % PEMs purity, as assessed by flow CD11b⁺F4/80⁺).

For confocal microscopy, cells (BMDM/PEMs) were seeded in Ibidi® chamber slides (µ-Slide 8 Well) at a density of 2×10^5 cell/well for 16 hours before being washed and stimulated. Cells were rinsed, fixed (PFA 4 % for 20 minutes at 4°C) and kept in PBS at 4°C for further investigations.

Cholesterol efflux. This was measured by an assay kit (MAK192, Sigma). BMDMs were stimulated for 24 hours with oxLDL (50µg/ml) and TDB (10µg/ml) in complete medium. Cells were then gently washed with warm medium (without FBS), and incubated with equilibration solution (containing the fluorescent cholesterol) overnight at 37°C. To induce cholesterol efflux, cells were washed and incubated with warm medium-containing Human

purified HDL (Abserotec, 50µg/ml), mouse serum (Sigma, 5% of final volume) or medium (without FBS). After 4 hours, supernatants were removed and cells were lysed with lysis buffer. Fluorescence of the supernatant and lysates were analyzed by VICTORX3 Plate Reader (Perkin Elmer). Cholesterol efflux was calculated as follows: $\text{efflux} = (\text{MFI supernatant} / \text{MFI cell lysate})$; % of efflux specific of the acceptor = $(\text{efflux with acceptor} / \text{efflux without acceptor}) * 100$.

Flow cytometry. Cell analysis. Spleen cell suspension, obtained after meshing and red blood cell lysis, as well as BMDMs or PEMs were incubated with Fc block solution (ebiosciences, clone 93, dilution 1/200 in flow buffer [PBS, 1 % BSA, 2 mM EDTA, 0.01 % NaN₃]) for 10 minutes at 4°C. Cells were then stained with fluorescently labeled anti-mouse antibodies, diluted in flow buffer at indicated concentration (Table I in the online-only Data Supplement) for 30 minutes at 4°C, prior to extensive wash and flow cytometry analysis. For neutral lipid staining, single cell suspensions of BMDMs were pelleted in PBS, resuspended with Bodipy® 493/503 (100 µM) diluted in PBS and incubated for one hour at 4°C. Cells were extensively washed in PBS and analyzed by flow cytometry.

Cytokine titration. Cytokines were titrated in cell supernatant according to manufacturer instructions using Cytometric bead assay (CBA) kits from BD biosciences: Mouse inflammation (Il-6, Ccl-2, Il-10, Tnf-α) and FlexSet Il-1α and Il-1β. No Il-12p70 or Ifnγ were found in supernatants from BMDMs and

PEMs. Titration of Csf1 in culture supernatant was performed according to the manufacturer instructions (DuoSet R&Dsystem).

Flow cytometer. The cytometric acquisition was performed on a LSR II Fortessa (BD biosciences) equipped with 4 lasers (405, 488, 561 and 640 nm). Cell analysis was done using BD FACSDiva Software 6.0 and figure-displayed dot plots and histograms were obtained using FlowJo software (TreeStar). CBA were analyzed using FCAP array v3.0.

Immunofluorescence. Cryosections (conserved at -80°C) were dried for 30 minutes, before being rehydrated in PBS for 10 minutes before the staining. Cryosections, as well as PFA-fixed cells, were then permeabilised in 0.1 % Triton X-100, 0.1 % Citrate buffer pH 6.0 (Dako) for 30 minutes. They were then washed in PBS, and incubated with the blocking solution (flow buffer + 5 % serum of secondary antibody species, i.e. goat or donkey) for 30 minutes, before being incubated with primary antibodies diluted in the blocking solution at indicated concentrations (Table II in the online-only Data Supplement) overnight at 4°C. Samples were extensively washed with PBS and incubated with secondary antibodies diluted in the blocking solution at indicated concentrations (Table II in the online-only Data Supplement) for 4 hours. Samples were again washed extensively in PBS, nuclei were counterstained with Hoechst 33342 (Invitrogen) and samples were mounted with CC mount™ (Sigma).

Apoptosis assay was performed using Roche In Situ Cell Death Detection Kit (Roche).

Sections of human coronary atherosclerotic plaque obtained by Patrick Bruneval, Paris, France, were collected after necropsy, were anonymized, and did not require specific ethics approval. The sections (paraffin-embedded) were rehydrated as follows: slides were heated at 50°C, dipped 3 minutes Xylene (2 times), 3 minutes in 50 % Xylene 50 % Ethanol 100 %, 3 minutes in Ethanol 100 %, 3 minutes in Ethanol 90 %, 3 minutes in Ethanol 70 % and 20 minutes in distilled water. Sections were incubated in antigen retrieval solution (Citrate buffer pH 6.0; Dako) at 95°C for 1 hour. Sections were washed in distilled water and incubated with in 0.1 % Triton X-100, 0.1 % Citrate buffer pH 6.0 (Dako) for 30 minutes before being immuno-stained following the same protocol described above. Masson's trichrome staining of human sections was performed according to manufacturer's instructions (Sigma, HT15-1KT).

Confocal analysis of samples was done using a Carl Zeiss LSM 700 confocal microscope and Zen2009 software. Epifluorescence analysis and brightfield imaging were done using Leica DM6000B microscope and analyzed with accompanying software. Images analysis was performed using Adobe Photoshop CS5 and ImageJ (NIH).

Quantitative real time polymerase chain reaction. RNA isolated from macrophages was prepared using an RNeasy mini kit (Qiagen). Isolated RNA (≥ 100 ng) was reverse-transcribed using QuantiTect Rev. Transcription Kit (Qiagen). Real-time PCR was performed on 5 μ l cDNA product (diluted 10 to 20 times) using SYBR Green qPCR mix (Eurogentec) on a Roche Lightcycler

and the primers described in Table III in the online-only Data Supplement (Sigma).

References:

1. Yamasaki S, Matsumoto M, Takeuchi O, Matsuzawa T, Ishikawa E, Sakuma M, Tateno H, Uno J, Hirabayashi J, Mikami Y, Takeda K, Akira S, Saito T. C-type lectin Mincle is an activating receptor for pathogenic fungus, *Malassezia*. *Proc Natl Acad Sci U S A*. 2009;106:1897-1902.
2. Iwawaki T, Akai R, Yamanaka S, Kohno K. Function of IRE1 alpha in the placenta is essential for placental development and embryonic viability. *Proc Natl Acad Sci U S A*. 2009;106:16657-16662.
3. Iwawaki T, Akai R, Kohno K, Miura M. A transgenic mouse model for monitoring endoplasmic reticulum stress. *Nat Med*. 2004;10:98-102.
4. Hartman MG, Lu D, Kim ML, Kociba GJ, Shukri T, Buteau J, Wang X, Frankel WL, Guttridge D, Prentki M, Grey ST, Ron D, Hai T. Role for activating transcription factor 3 in stress-induced beta-cell apoptosis. *Mol Cell Biol*. 2004;24:5721-5732.

Supplemental Figures

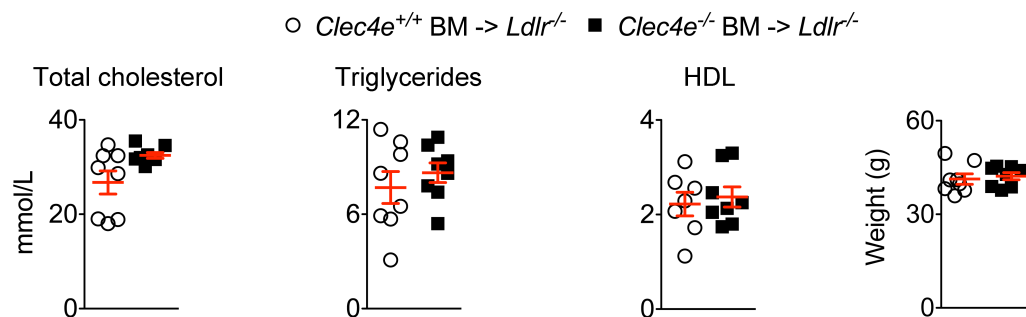


Figure I: Genetic deletion of *Clec4e* in bone marrow-derived cells does not change serum cholesterol, triglycerides, HDL-cholesterol, or weight of *Ldlr*^{-/-} mice under HFD for 20 weeks.

Total cholesterol, triglycerides and HDL plasma concentration (mmol/L), as well as weight (g) of mice from both groups of *Ldlr*^{-/-} mice after 20 weeks under HFD. No significant differences were observed between groups.

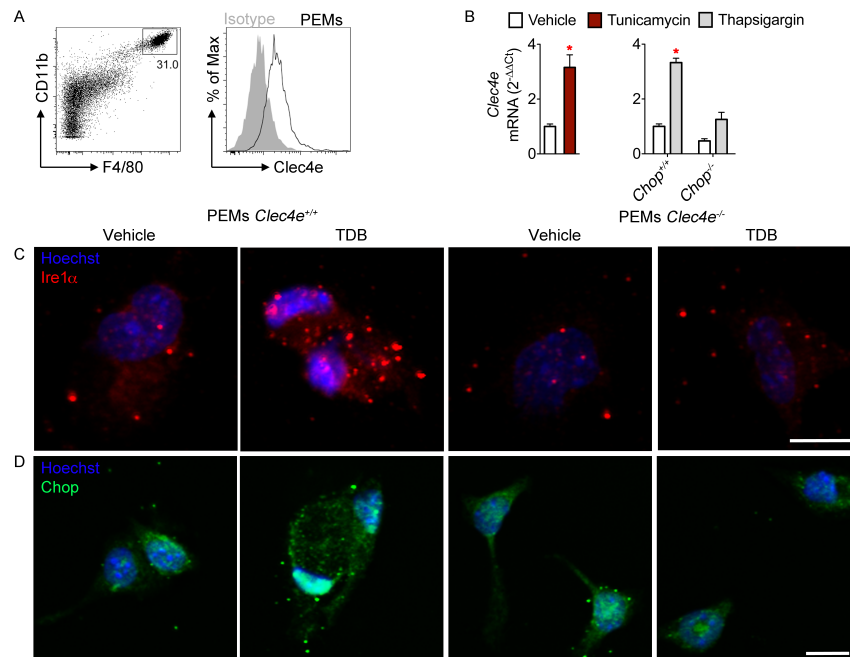


Figure II: ER stress induces Clec4e expression and Clec4e promotes ER-stress in PEMs.

A- Representative flow charts of Clec4e expression by PEMs (CD11b⁺F4/80⁺) *ex vivo*.

B- RT/Q-PCR analysis of *Clec4e* mRNA expression by BMDMs treated with or without tunicamycin (Left panel; *p<0.05, tunicamycin- vs vehicle-treated BMDMs) and of *Clec4e* mRNA expression by *Chop*^{+/+} and *Chop*^{-/-} BMDMs treated with or without thapsigargin for 12 hours (Right panel; *p<0.05, thapsigargin-treated *Chop*^{+/+} BMDMs vs all the other conditions). Data were obtained by using technical quadruplicates and are representative of 2 independent experiments. Kruskal-wallis with Dunn's post test.

C-D Representative images of Ire1α expression (C) and Chop distribution (D) in PEMs from *Clec4e*^{+/+} and *Clec4e*^{-/-} mice stimulated with TDB for 16 hours. Data are representative of 2 independent experiments (Scale bars: 10μm).

Clément, Necrotic sensor Clec4e promotes atherosclerosis

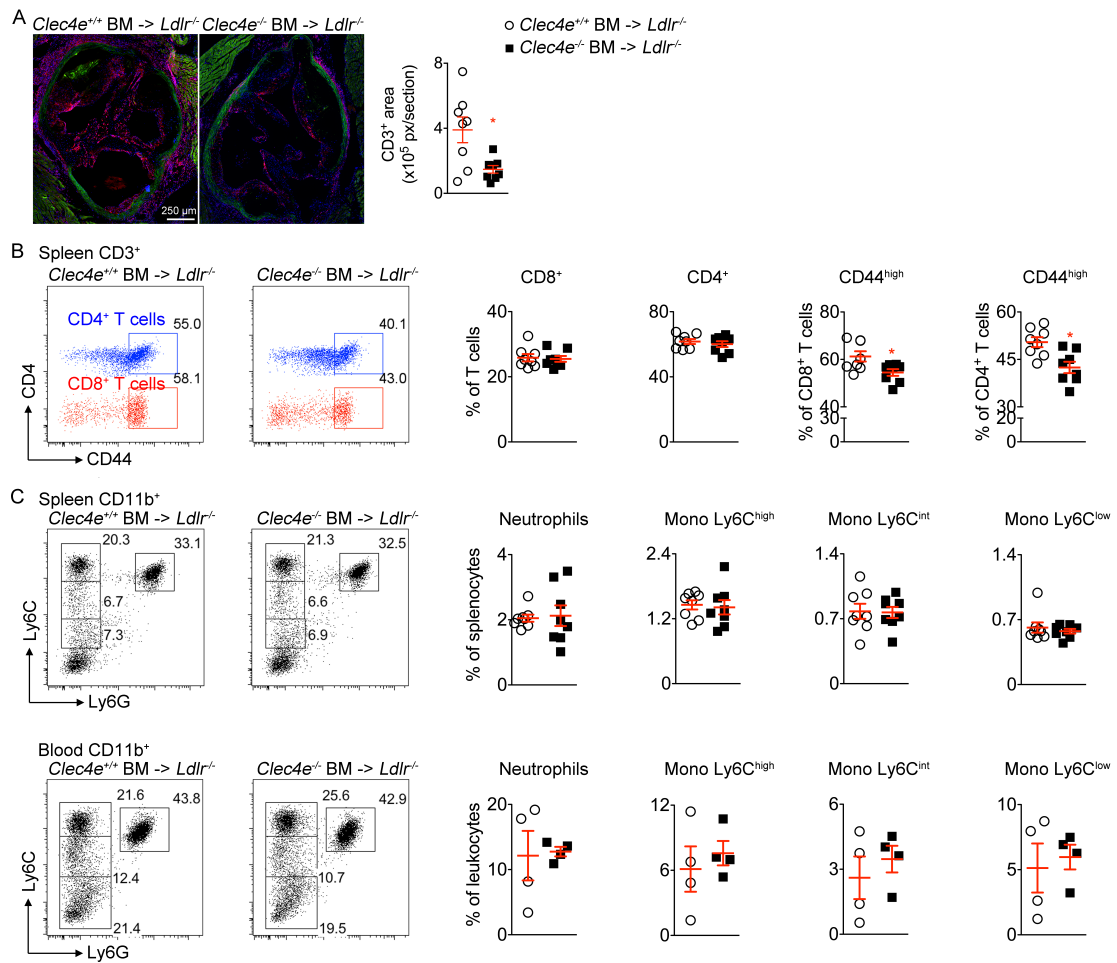


Figure III: Immunophenotypical analysis of spleen and lesions.

A- Fluorescent immunostainings for CD3 (red) on atherosclerotic plaques from *Clec4e*^{+/+} BM → *Ldlr*^{-/-} and *Clec4e*^{-/-} BM → *Ldlr*^{-/-} mice. Autofluorescence of the tissue is depicted in green (Elastin & myocardium).

B- Flow cytometry analysis of T cell distribution and activation (CD44⁺ expression) in the spleen of *Clec4e*^{+/+} BM → *Ldlr*^{-/-} and *Clec4e*^{-/-} BM → *Ldlr*^{-/-} mice.

C- Flow cytometry analysis of myeloid cell distribution (neutrophils and monocytes Ly6C^{high}, ^{int}, ^{low}) in the spleen and blood of *Clec4e*^{+/+} BM → *Ldlr*^{-/-} and *Clec4e*^{-/-} BM → *Ldlr*^{-/-} mice.

*p<0.05, n= 8 mice/group, Mann-Whitney test (A, B).

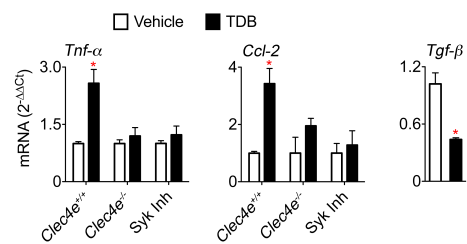


Figure IV: Clec4e/syk axis stimulates *Tnf-α* and *Ccl-2* but inhibits *Tgf-β* mRNA expression in BMDMs.

RT/Q-PCR analysis of *Tnf-α*, *Ccl-2* and *Tgf-β* mRNA expression by *Clec4e*^{+/+} and *Clec4e*^{-/-} BMDMs treated with or without TDB for 12 hours, in the presence or not of Syk inh. *p<0.05, TDB- vs untreated *Clec4e*^{+/+}, Kruskal-wallis with Dunn's post test. Data were obtained using technical quadruplicates and are representative of 2 independent experiments.

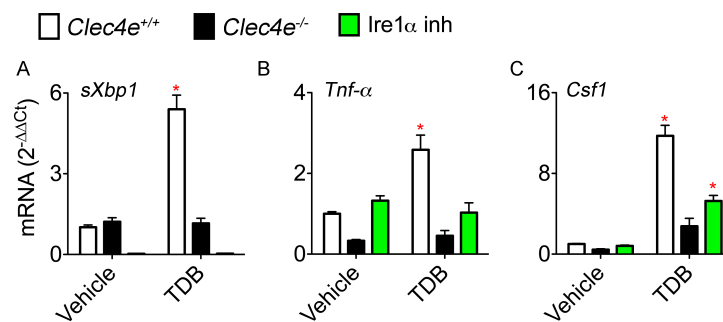


Figure V: Pharmacological inhibition of Ire1 α endonuclease activity impairs Clec4e signaling in macrophages.

RT/Q-PCR analysis of *sXbp1*, *Tnf- α* and *Csf1* mRNA expression by *Clec4e*^{+/+} and *Clec4e*^{-/-} BMDMs treated for 12 hours with or without TDB, in the presence or not of the Ire1 α inh. *p<0.05, TDB- vs vehicle-treated *Clec4e* BMDMs, Kruskal-wallis with Dunn's post test. Data were obtained using technical quadruplicates and are representative of 2 independent experiments.

Panel	Target	Clone	Fluorochrome	Compagny
MINCLE on PEMs				
	CD11b	M1/70	Alexa fluor® 488	eBiosciences
	F4/80	BM8	PE-Cy7	eBiosciences
	Clec4E	4E9	APC	Home-made
CD36 on BMDMs				
	CD11b	M1/70	Alexa fluor® 488	eBiosciences
	CD36	No.72-1	APC	Biolegend
Spleen T cells				
	CD3	145-2C11	Alexa fluor® 488	Biolegend
	CD4	RM4-5	Pacific Blue	Biolegend
	CD8	53-6.7	PerCP	Biolegend
	CD44	1M7	APC	Biolegend
Blood/Spleen myeloïd cells				
	CD11b	M1/70	Alexa fluor® 488	eBiosciences
	Ly6C	7/4	PE	Abserotec
	Ly6G	Gr1	Pacific Blue	Biolegend
PEMs ABCA1				
	ABCA1	5A1-1422	A647	Abserotec

Table I: Antibodies used for flow cytometry.

Target	Host species	Clone (Isotype)	Working dilution	Compagny (Cat n°)
Mouse				
Clec4e	Rat	4E9 (IgG1)	1/50	MBL (D292-3)
Atf3	Rabbit	polyclonale (IgG)	1/200	Sigma (HPA001562)
p21 ^(Waf1, Cip1)	Rabbit	polyclonale (IgG)	1/200	eBiosciences (14-6715)
Ire1 α	Rabbit	14C10 (IgG)	1/100	Cell signaling technology (#3294)
Ki67	Rabbit	D3B5 (IgG)	1/200	Cell signaling technology (#9129)
pSyk (Y323)	Rabbit	polyclonale (IgG)	1/100	Cell signaling technology (#2715)
MOMA-2	Rat	MOMA-2 (IgG2b)	1/200	Abserotec (MCA519)
Chop	Rabbit	polyclonale (IgG)	1/200	SantaCruz (sc-575)
CD68	Goat	polyclonale (IgG)	1/100	SantaCruz (sc7084)
Il-1 β	Rabbit	polyclonale (IgG)	1/200	Abcam (ab9722)

Human				
CLEC4E	mouse	15H5 (IgG2b)	1/50	Invivogen (mabg-hmcl)
MPO	Rabbit	polyclonale (IgG)	1/200	DAKO (A0398)
Secondary antibodies				
Rabbit IgG (Alexa Fluor® 555)	Donkey	polyclonale	1/200	Thermo fisher scientific/Invitrogen (A-31572)
Rat IgG (Alexa Fluor® 488)	Goat	polyclonale	1/200	Thermo fisher scientific/Invitrogen (A-11006)
Rat IgG (TRITC)	Goat	polyclonale	1/200	Thermo fisher scientific/Invitrogen (A18870)
Mouse IgG (Alexa Fluor® 647)	Goat	polyclonale	1/200	Thermo fisher scientific/Invitrogen (A-21235)

Table II: Antibodies used for immunofluorescence.

Inflammation	Forward primer 5'->3'	Reverse primer 5'->3'
<i>Ubc</i>	CACCAAGAAGGTCAAACAGGA	CCCAAGAACAAGCACAAGG
<i>Clec4e</i>	CCCACCACACAGAGAGAGGA	AGTTCTGCCCCGGAAATTTGA
<i>Csf1</i>	GAACAAGGCCTGTGTCCGAA	CTGCTAGGGGTGGCTTTAGG
<i>Tnf-α</i>	GGTCCCCAAAGGGATGAG	CACTTGGTGGTTTGCTACGAC
<i>Ccl-2</i>	GTTAACGCCCCACTCACCT	TTCTTTGGGACACCTGCTG
<i>Tgf-β</i>	GCAACATGTGGAAGCTCTACCAG	CAGCCACTCAGGCGTATCA
Proliferation		
<i>Klf4</i>	CCCACACTTGTGACTATGCAGG	GGCGAATTTCCACCCACAGC
<i>Myc</i>	TTCCTTTGGGCGTTGGAAAC	GCTGTACGGAGTCGTAGTCG
<i>cMaf</i>	GCAGGTAGACCACCTCAAGC	TCGGGAGAGGAAGGGTTGTC
<i>Maf-b</i>	GGCAACTAACGCTGCAACTC	ACGGAAGGGACTTGAACACC
Cholesterol efflux		
<i>Abca1</i>	CGAGGCTCCCGGTGTTG	GGCTGTACAGAAGAAGCCTCTGA
<i>Abcg1</i>	TCACCCAGTTCTGCATCCTCTT	GCAGATGTGTCAGGACCGAGT
ER stress		
<i>Xbp1</i>	TACGGGAGAAAACCTCACGGC	CTTACTCCACTCCCCTTGCC
<i>sXbp1</i>	AGCTTTTACGGGAGAAAACCTCA	GCCTGCACCTGCTGCG
<i>Chop</i>	CGGCCTGGGAAGCAACGCAT	GTCGATCAGAGCCCCGCCGTG

Table III: Primers used for Q-PCR.